

Exploration of power take off in wave energy converters with two-body interaction

Hao Wang^{*1}, Khairil Sitanggang^{2a} and Jeffrey Falzarano^{1b}

¹Department of Ocean Engineering, Texas A&M University, College Station, USA

²INTECSEA Inc, Worley Parsons Group, Houston, USA

(Received February 19, 2017, Revised May 27, 2017, Accepted June 2, 2017)

Abstract. The study explores a novel design of wave energy converter (WEC) that utilizes the interaction between an inside heaving vertical cylinder with an outside fixed hollow cylinder. This design originates from the oscillating water column (OWC) type WEC but replaces the pneumatic power take off (PTO) through the Wells turbine with the hydrodynamic PTO through the inside heaving cylinder. To effectively evaluate the maximum power output, the system has been modeled in the hydrodynamic software AQWA (developed by ANSYS Inc) that has accumulated extensive offshore industry users. Ranges of the PTO parameters have been examined to make sure that proper linear damping can be implemented to simulate the PTO force. Comparing the efficiency of the pneumatic PTO with the hydrodynamic PTO, it appears that the hydrodynamic PTO is more promising than the traditional Wells turbine for an OWC system.

Keywords: power take off; two-body interaction; oscillating water column; damping; AQWA; point absorber

1. Introduction

Ocean wave energy, a form of high-density renewable energy resource, distributes abundantly in the coastal area where concentrates majority of the world's population and industry (Falzarano *et al.* 2012). In the past decades, scientists and engineers from both academia and industry have been continuously making their efforts to innovate, develop and optimize wave energy converters (WECs) of all sorts (Drew *et al.* 2009). Oscillating water column and point absorber are two types of these designs that attract interests from a great many WEC developers.

Oscillating water column (OWC) type WEC consists of two modules: (a) the energy concentration module, which is the hollow structure to concentrate the water column heave motion through its interaction with the wave field; (b) the pneumatic power take off module, including the air chamber above the waterline and the (Wells) turbine installed at the top of the chamber to convert the airflow to electricity (Falnes 2002 and Wang 2013).

*Corresponding author, Professor, E-mail: haowang8901@gmail.com

^a Dr., Email: ksitanggang@aggienetwork.com

^b Professor, Email: jfalzarano@civil.tamu.edu

Point absorber (PA) extracts energy from the heave motion of a floating body riding the wave (Cho *et al.* 2012). Mechanism to convert floating body motions to electricity in point absorber type WECs varies in different designs (López *et al.* 2013). This study focuses on the application of the hydrodynamic PTO similar to the linear generator buoy developed by Oregon State University (OSU) as summarized by Schwartz and Mentzer (2016). Linear direct power PTO is superior in that it requires only one moving structure which reduces mechanical complexity and that it can be damped electronically (Bard and Kracht 2013).

Marine Dynamic Laboratory (MDL) in Texas A&M University are inspired to look at the combination of the OWC and the PA that both utilize the heave motion. Fig. 1 is the MDL WEC studied in this paper.

To show the differences between the MDL WEC with other WEC designs, similar WEC designs are listed in Table 1. The uniqueness of the MDL concept is that it adopts two floating (not fully submerged) bodies interacting with waves.

Table 1 Concepts comparison

Concepts/ Organizations	Wave Interacting	Floating Status	PTO	Main Geometry
MDL	Two Bodies	Floating-Floating	Linear Direct	Tube
OSU PA	One Body	Floating	Linear Direct	Cylinder
OPT PB3	One Body	Floating	Mechanical	Spar
OWC	One Body	Floating	Pneumatic	Tube
AQUABuOY	Two Bodies	Floating-Submerged	Hydraulic	Tube
IPS Buoy	Two Bodies	Floating-Submerged	Hydraulic	Cylinder
2-Body WEC	Two Bodies	Floating-Submerged	Mechanical	Cylinder

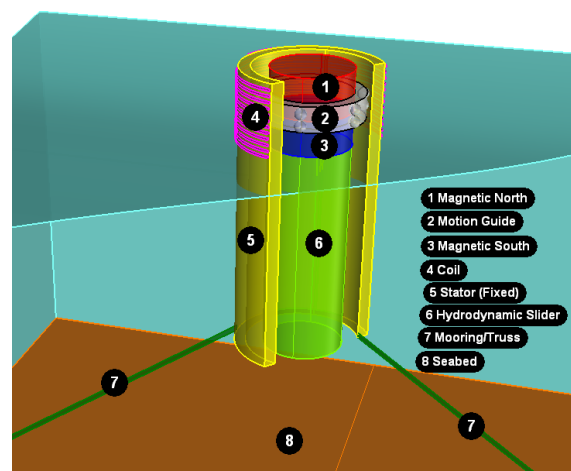


Fig. 1 Concept of oscillating buoy

Considering that the wave-structure interaction is most significant near the free surface, two floating bodies yield more significant wave-structure interaction. Utilization of the relative motion between the two floating bodies has also been studied by Cho and Kim (2017) but their design is closer to a combination of two point absorbers (PAs). The geometry of the MDL WEC is similar to AquaBuOY. However, the slider in the MDL WEC is a much larger floating cylinder while AquaBuOY uses a hose pump.

The most typical analysis procedure with potential theory is: (1) Perform frequency domain analysis (Guha 2016, Liu and Falzarano 2016) on the WEC. For multi-body WEC, include the multi-body interactions (Liu and Falzarano 2017). After frequency domain analysis we get the added mass, (potential) damping, response amplitude operators (RAOs) and drift forces; (2) Perform time domain analysis (Somayajula and Falzarano 2015) on the WEC, which uses the outputs from the previous frequency domain analysis. After time domain analysis we get the responses of the WECs in the irregular sea-state.

The focus of this paper is to implement the hydrodynamic PTO to the traditional oscillating water column (OWC) WEC. Both the MDL concept and OWC concept extract energy from the piston mode (heaving up and down) of the water inside the hollow cylinder. Molin (2001) has studied the piston mode of the moonpool theoretically and given the approximation for its natural frequencies. Experimental studies have been conducted for a cylindrical moonpool (independent hollow cylinder) by Garriga and Falzarano (2008) and for squared moonpool (inside a floating structure) by Yang *et al.* (2016). In general, the moonpool or moonpool-like shape can amplify the heave motion of water (relative to the heave motion of water induced by the incident wave), which can improve the efficiency of the WECs. Evaluating the potential to convert the piston mode to electricity in a more accurate and standard way is a key target in the WEC development.

To standardize our analysis, simulations are conducted with AQWA (developed by ANSYS Inc) extensively used in the offshore industry. The pneumatic PTO involves oscillating air pressure that cannot be modeled in AQWA directly. Alternatively, the wave potential around an OWC system has been accurately solved by Evans and Porter (1997). Using their solutions, under certain assumptions (Wang and Falzarano 2013), a Matlab program has been developed to model the pneumatic OWC. The Matlab program has been successfully validated by a method called control boundary wave integration (Wang and Falzarano 2017). The method reveals that the energy deficit in the 3-D wave field strictly matches the energy output through the pneumatic turbine. To make fair comparison, in AQWA analysis, identical design parameters (like the draft and overall diameter) and sea state are used.

2. Analysis inputs and procedure

AQWA, including many modules (like AQWA-LINE, AQWA-LIBRIUM and AQWA-DRIFT), is a prestigious engineering analysis suite. In particular, the suite includes:

AQWA-LINE: calculates the wave loading as well as the responses of bodies when they are exposed to regular wave. First order wave forces and second order wave drift forces are calculated in the frequency domain (ANSYS Inc 2011a).

AQWA-DRIFT: simulates the real-time motions of a floating body or bodies in irregular waves. AQWA-DRIFT does not work for regular wave, and that's why we used AQWA-NAUT for the regular wave cases. When more than one body is studied, coupling effect between bodies may be considered (ANSYS Inc 2011b).

Table 2 Parameters for an OWC system

Variable	Value	Units
Buoy Radius 1	2.40	m
Buoy Radius 2	3.25	m
Overall Radius	3.66	m
Common Draft	10.97	m
Common Height	16.00	m
Cylinder Mass 1	2.040×10^5	kg
Cylinder Mass 2	3.741×10^5	kg
Outer Mass	5.242×10^4	kg
Common VCG below the water line	-6.00	m
Volume of the air chamber (when the air turbine is used)	211.3	m ³

AQWA-NAUT: simulates the real-time motions of a floating body or bodies in regular or irregular waves. Nonlinear Froude-Krylov and hydrostatic forces are estimated under instantaneous incident wave surface. When more than one body is studied, coupling effects between bodies may be considered (ANSYS Inc 2011c).

HYDI (hydrodynamic interaction): activates the interaction effects between structures. This option is usually used in AQWA-LINE. FIDD (frequency independent diagonal damping): inputs a diagonal linear damping, which is added to the (linear) potential damping calculated by AQWA-LINE. MDIN (Morrison drag input): inputs the hull drag force for a diffracting structure. ZRON (z coordinate relative to wave surface print on): outputs the z coordinate relative to the wave surface, which can be used to output the wave elevation time series.

The theoretical illustrations can be found in the AQWA User Manuals (ANSYS Inc, 2011a,b,c). The format of inputs can be found in the AQWA Reference Manual (ANSYS Inc 2012).

Table 2 shows the input parameters in AQWA-LINE (the frequency domain module). The inside cylinder is floating (by default), so its mass matches its displacement. Mass of the outside body is also equivalent to its buoyancy (it is not very important since in time-domain its 6 degrees of freedom are locked). For the hydrodynamic PTO, inside cylinders with different radii are tested in the study. In AQWA-LINE, wall thickness of the outside hollow cylinder cannot be zero. Therefore, we modeled the wall of 0.25 m thickness, which is the unit length in panelization. Outer radius 3.80 m and inner radius 3.55 m of the wall averages 3.675 m, which has just 0.4% difference from the pneumatic OWC model in Matlab.

Fig. 2 shows the panel model in AQWA with the mesh size of 0.25 m. In both Fig. 2(a) and Fig. 2(b), the outside hollow cylinder is fixed and the inside cylinder is the moving part. We adopted the panel size of 0.25 m, which means unit mesh should be 0.25 m \times 0.25 m square. Considering the general dimensions of the system (7.32 m diameter and 16.0 m height), the panel size is small enough for our analysis. In practice, when the radius of the inside body becomes too close to the radius of the outside body (for example 0.1 m), some warnings will be given due to the limitations

of the software. In order to get a good approximation of the potential (maximum power output) of the hydrodynamic PTO, the radius of the inside cylinder in Fig. 2(b) is set to 3.25 m to avoid those warnings. In this way, the maximum power output calculated for the hydrodynamic PTO may be conservative (radius smaller than the ideal situation). This actually does not affect the engineering estimation we will make as the comparisons are expressed with inequalities (for example, ">14%").

The two-body interaction is activated by using the HDYI option in AQWA-LINE. Frequency domain analysis is necessary before time domain analysis as it provides the response amplitude operator (RAO), added mass, radiation damping and drift force coefficients. Fig. 3 are the RAOs of the inside cylinders with different radii under the same linear damping 4×10^4 N/(m/s). Fig. 3 shows that the amplification of heave motion in certain frequency range, especially significant within $0.7\text{rad/s} \sim 0.9\text{rad/s}$. The cylinder with larger radius shows greater potential to work under load (modeled as linear damping).

The sea state is obtained from the NOAA Station 44013, the closest station to Boston. Wave heights and wave periods (daily from Nov 11, 2015 to Nov 10, 2016) at this station have been averaged as the simulation sea state (Wang and Falzarano 2017). It is selected on observation of its relatively mild wave height, wave length and water depth. The average wave height is 0.93 m, the average period is 7.68s, and the water depth is 64.5 m. The Matlab model can only solve regular wave, so the in-line comparison is AQWA-NAUT simulation using regular incident wave.

In time domain simulations, the outside body is fixed. In AQWA-DRIFT, this is achieved by using the DACF option to deactivate all six degrees of freedom for the outside body. Similarly, the inside body has only one degree of freedom (heave). The two bodies have no relative motion except for the heave. This situation can be expensive in large water depth, so the cases are setup in shallow water location. (In general, the cost to keep a floating structure fixed will increase with the water depth. One reason is that larger water depth means more investments for the mooring system. Another reason is that the shallow water area is usually closer to the coast, which implies less cost of maintenance, less severe sea state and so on.)

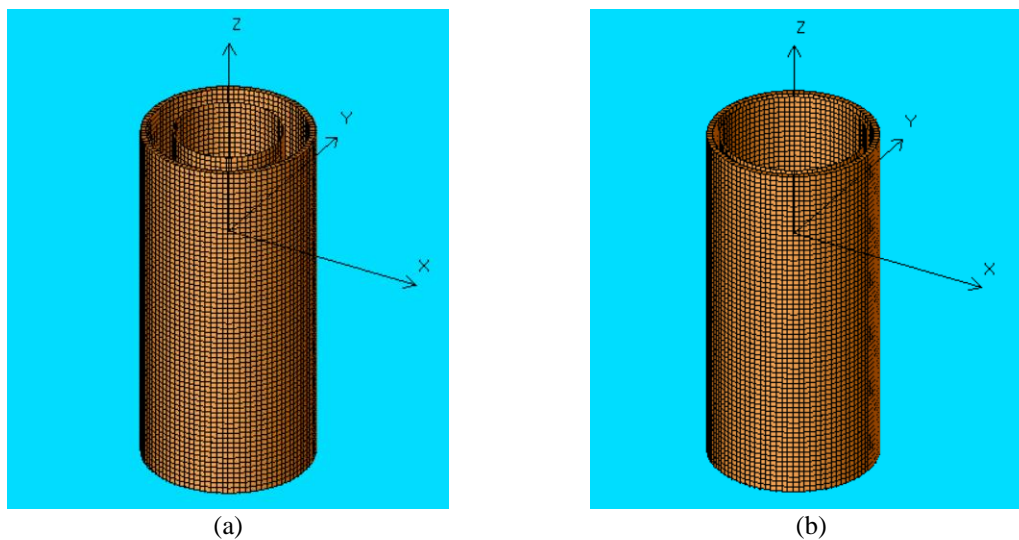


Fig. 2 Panel model of the two-body system in AQWA

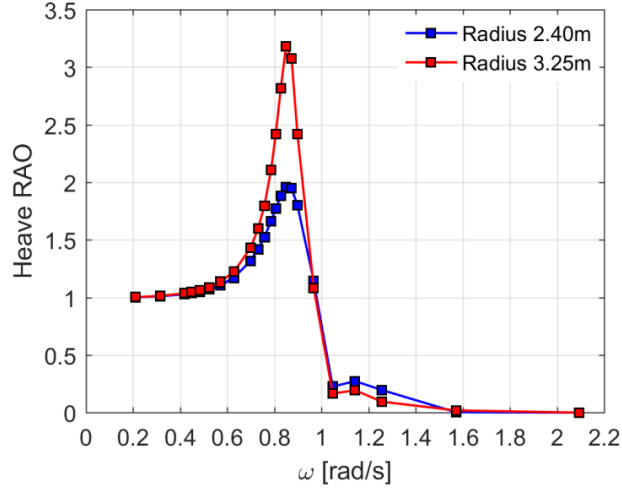


Fig. 3 Buoy heave RAO under the same damping

The equation of heave for the oscillating buoy is

$$(m + m_a)\ddot{z}(t) + B\dot{z}(t) + \frac{1}{2}\rho AC_{dv}\dot{z}_{rel}(t)|\dot{z}_{rel}(t)| + (K_h + K_a)z(t) + F_R(t) = F_e(t) \quad (1)$$

Note this equation is not valid for irregular waves, for which Cumming's equation needs to be used.

- 1) m is the mass, m_a is the heave added mass;
- 2) B is the linear damping for heave; in time domain it is usually put to represent external damping. In this study, we try to simulate the useful electromagnetic load as the linear "damping". Section 3 will show that under certain conditions, the term 5) $F_R(t)$ can be modeled as a linear damping so we can omit the term 5) $F_R(t)$ in that case.
- 3) C_{dv} is the quadratic viscous damping coefficient; $\dot{z}_{rel}(t)$ is the heave speed relative to fluid particles; A is the projected area (in z direction) of the inside cylinder;
- 4) K_h is the hydrostatic stiffness; K_a is the additional stiffness due to the spring system which may be implemented to position the oscillating buoy. In primary design phase, K_a is set as zero;
- 5) $F_R(t)$ is the resistant force from the PTO system; the next section will justify that under certain conditions, the hydrodynamic PTO (electromagnetic force) can be modeled as linear damping. That not only provides the convenience in modeling the system with AQWA, but also serves as an efficient way of evaluating the power output.
- 6) $F_e(t)$ is the hydrodynamic exciting force.

Table 3 shows the implementation of different terms/variables in the AQWA suite. The terms marked as "Manual input" are the ones that we need to input. Additional stiffness (for further optimization) is not implemented at this stage.

The nonlinear part of the PTO (if any) cannot be modeled appropriately in AQWA because the quadratic damping in AQWA is quadratic to the relative speed (relative to the fluid velocity). In the following section, some numerical tests are conducted to make sure linear PTO is dominating.

3. Load linearization

This section is to justify that the electromagnetic force can be roughly modeled as a linear damping in the simulations (Zheng *et al.* 2015). This practice is applicable only under certain parameters in both hydrodynamic (wave and floating cylinder) aspect and electromagnetic aspect (generator) of the MDL WEC. To simplify the problem and make the linearization of the electromagnetic force possible, a single-phase generator is discussed in this study. This setting and the following modeling are acceptable since the focus of the study is the potential (maximum power output) of the WEC. The basic magnetic field in the generator has been discussed by Thorburn and Leijon (2007) and the magnetic flux in the system can be expressed as

$$\Phi(t) = \Phi_t M[z(t)] \quad (2)$$

Φ_t is the magnitude of the magnetic flux, which is a constant determined by the hydrodynamic PTO system. Function $M(z)$ is the generalized relationship between the magnetic flux and the position of the slider. To linearize the electromagnetic force, we have modified the cosine form of $M(z)$ provided by Thorburn and Leijon (2007) into

$$M(z) = \sin[\gamma(z - z_0)] \quad (3)$$

z_0 is the initial position of the COG for the inside buoy, normally it should be set as the equilibrium position of the buoy. γ is the rate of magnetic field strength variation in the generator. As we can design the generator (magnetic field) differently and set the equilibrium position z_0 where the magnetic flux change is sensitive to the heave motion, the electromagnetic field in Eq. (3) can be realized. Corresponding to a given PTO, $M(z)$ can have other input parameters but the only variable is the position $z(t)$ of the slider. Using Faraday's law, the voltage in the circuit is

$$U(t) = -\frac{d\Phi}{dt} = -\Phi_t \frac{dM}{dz} \dot{z}(t) \quad (4)$$

The form of $U(t)$ can be more complex depending on the form of $M(z)$ function, however, it's linear to the vertical velocity $\dot{z}(t)$. In irregular sea-state, $U(t)$ has multiple frequencies, however, using the fast Fourier transform (FFT), $U(t)$ can be decomposed into

$$U(t) = \sum_{j=1}^N U_j \cos(\omega_j t + \phi_j) \quad (5)$$

N is the number of time steps in the time history.

Fig. 4 shows that FFT effectively decomposes the irregular voltage time series into many sinusoidal signals (red dots). The generator circuit can be complex but it must be a RL circuit composed by the total resistance R and the total inductance L . The inductance L is not negligible in any alternating current (AC) circuit. The voltage and the current can always be superpositioned. For each single frequency (ω_j) voltage signal $U_j(t) = U_j \cos(\omega_j t + \phi_j)$, the corresponding current $I_j(t)$ is

$$I_j(t) = \frac{U_j(t)}{R + \omega_j L i} = \frac{U_j}{\sqrt{R^2 + \omega_j^2 L^2}} \cos(\omega_j t + \phi_j + \varphi_j) \quad (6)$$

In which φ_j is the phase variation induced by the inductance L

$$\varphi_j = -\tan^{-1}\left(\frac{\omega_j L}{R}\right) \quad (7)$$

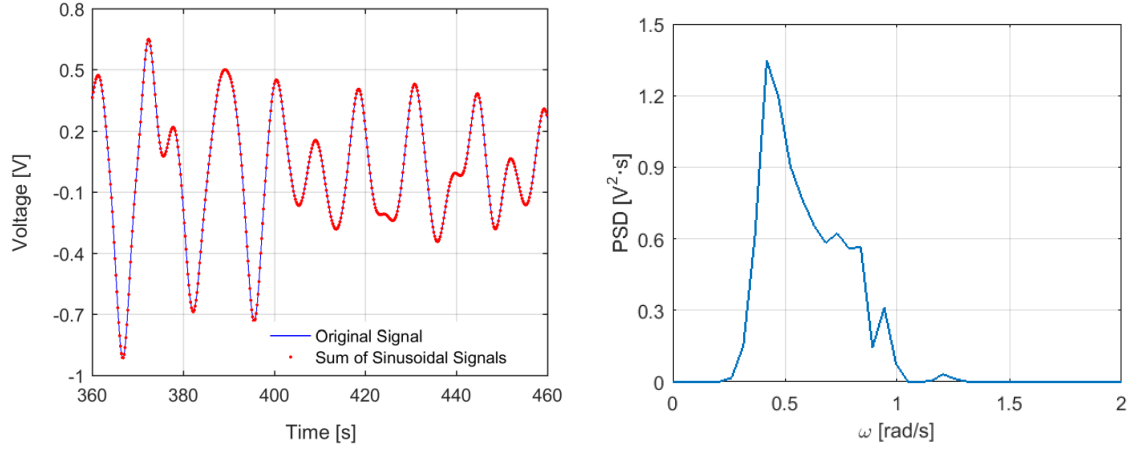


Fig. 4 FFT in decomposing the voltage signals

The total current in the circuit is

$$I(t) = \sum_{j=1}^N I_j(t) \quad (8)$$

The instantaneous power in the circuit is

$$P(t) = U(t) \cdot I(t) \quad (9)$$

According to the conservation of energy, the output power comes from the heaving cylinder working under the vertical electromagnetic force $F_R(t)$, so at any instant

$$F_R(t) = \frac{U(t) \cdot I(t)}{\dot{z}(t)} \quad (10)$$

Combinations of the resistance R and the inductance L are examined for random motions of the oscillating buoy. Using the actual heave motion and velocity time series, we can check the linearity of the resistant force $F_R(t)$ versus the vertical velocity $\dot{z}(t)$. Fig. 5 is the linear regression for 6000 steps of $F_R(t)$ versus $\dot{z}(t)$. Linear regression results printed in Fig. 5-7 are interpreted as follows:

- (1) R square: represents the percentage of data variability that can be explained by the linear regression. In these tests, 0.90 is considered as the minimal limit that linear damping is applicable;
- (2) Slope: since the velocity and the resistant force have been normalized (by their maximum values), ideally the slope of line fitting should be 1. Slope other than 1 indicates nonlinearity;
- (3) p value: the p value of the slope represents the confidence of the linear regression. 0% means complete affirmative on linear regression but it is always fulfilled more easily than (2). As it's always zero, it is printed in Figs. 6 and 7.

These criteria help us judge whether the correlation between the electromagnetic force and the velocity is linear. Actually, it is also necessary to observe the scatter diagram because sometimes the regression numbers as criteria are not strict enough.

In Fig. 5, though the resistant force is not strictly linear to the vertical velocity, it is generally acceptable to model it as a linear damping force to simplify the simulation.

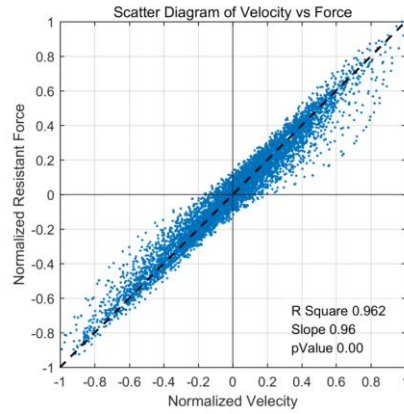
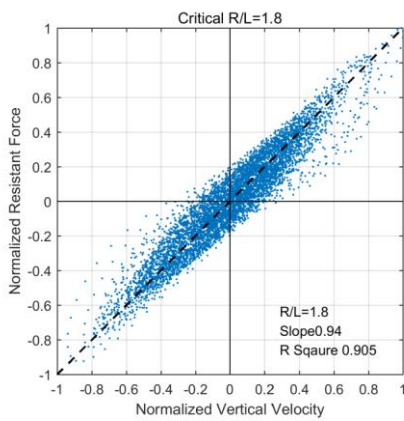
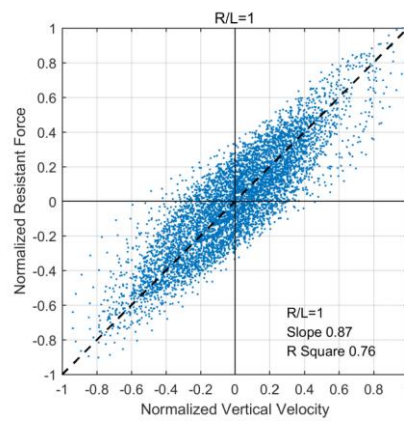


Fig. 5 Linear regression of time history (linear)

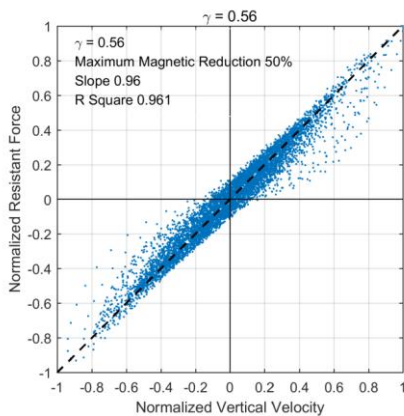


(a)

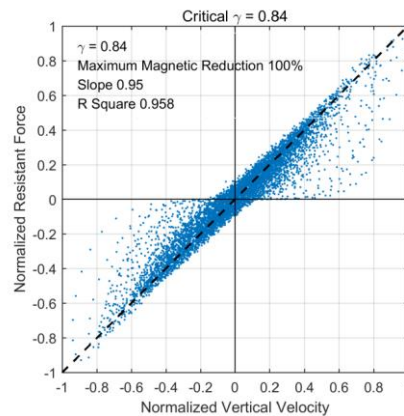


(b)

Fig. 6 Linear regression of time history (a:acceptable, b:non-linear)



(a)



(b)

Fig. 7 Linear regression of time history (a:acceptable linear, b:non-linear)

Table 4 Sensitivity tests on different parameters

Case	Hydrodynamic Buoy			Seed	Generator		Regression	
	H_S	ω_p	B		γ	R/L	slope	R^2
1(b)	2.0	0.419	5.00×10^4	1	0.5	3	0.96	0.962
1(r)	2.0	0.419	5.00×10^4	22	0.5	3	0.96	0.961
2	2.0	0.419	2.00×10^4	1	0.5	3	0.95	0.955
3	2.0	0.419	2.00×10^5	1	0.5	3	0.97	0.973
4	3.0	0.419	5.00×10^4	1	0.5	3	0.94	0.960
5	2.0	0.818	5.00×10^4	1	0.5	3	0.94	0.933

Table 4 shows a series of sensitivity tests conducted on different parameters. Compared with the base case 1(b), other cases change one variable at one time (i.e., seed number, linear damping, wave height and peak frequency). The varying parameters in Table 4 (except R/L and γ) are not dominating in creating nonlinearity in the tested range.

Nonlinearity is closely related to the R/L value of the circuit and the rate of the magnetic field strength variation γ in the generator. The following are some numerical tests for the R/L critical value. $R/L=1.8$ (in Fig. 6(a)) is the critical (last acceptable) value when the linear damping modeling is considered as applicable. Fig. 6(b) shows that when $R/L=1$, slope and R square are not very satisfying, evident by that many data points fall apart from linear correlation (dashed line).

The other important parameter is γ that represents the variation rate of magnetic strength with the buoy position. Sine form of magnetic strength function $M(z) = \sin[\gamma(z - z_0)]$ is assumed tentatively. If the actual magnetic field is different, it should also be examined.

Fig. 7(a) is the critical (last acceptable) value for γ . In fact, $\gamma > 0.56$ doesn't seem to satisfy linear damping assumption (see Fig. 7(b)). In the tested cases, $\gamma=0.56$ leads to $\pi/3$ maximum magnetic phase which means maximum 50% drop in magnetic field strength, and $\gamma=0.84$ leads to $\pi/2$ maximum magnetic phase which means maximum 100% drop in the magnetic field strength.

These tests should be performed prior to time domain analysis to make sure that the hydrodynamic PTO can be modeled as linear damping. Linear damping is input with the FIDD card in AQWA-NAUT (ANSYS Inc 2011c).

4. Viscous damping discussions

Besides the "useful" linear damping that we can design, other forms of damping needs to be accounted in the simulations (see Table 3).

Potential damping is associated with the radiated waves and that is why it's also named radiation damping. It is calculated in AQWA-LINE and can be passed on to AQWA-DRIFT or AQWA-NAUT automatically.

Hydrodynamic software built from the potential flow theory needs to approximate the viscous effect in some way, for instance, using the Morrison elements. Usually model tests are necessary to determine the linear and quadratic part of viscous damping (Cozijn *et al.* 2005). The linear part of

viscous damping originates from frictions, and the quadratic part of viscous damping is induced by the drag. Quadratic viscous damping is related closely to the Keulegan-Carpenter (KC) number

$$KC = \frac{2\pi A_z}{D} \quad (11)$$

A_z is the amplitude of heave motion, D is the diameter of the heaving cylinder. According to the Morrison's equation, the heave quadratic damping force of an oscillating vertical cylinder is

$$F_D = \frac{1}{2}\rho C_{dv} A \dot{z}_{rel}(t) |\dot{z}_{rel}(t)| \quad (12)$$

There are many model tests that measured C_{dv} in different KC range (Tao *et al.* 1999). Thiagarajan and Troesch (1994) have tested a range of KC that can reasonably cover our cases. According to their tests, when $KC \in [0,1]$, C_{dv} monotonically decreases with respect to KC and converges to 1.6 as KC goes to 1. In the cases studied, $KC \in [0.58,1.06]$ means that $C_{dv} \leq 1.6$. As a conservative estimation on the quadratic damping coefficient, set $C_{dv} = 2.0$ (25% margin on top of $C_{dv} = 1.6$). Time domain simulations using this "over-estimated" quadratic damping should otherwise have larger heave and larger KC , thus the actual C_{dv} should be smaller than 2.0. By setting C_{dv} at larger value, the viscous damping effect is never underestimated. The term $\frac{1}{2}\rho C_{dv} A$ needs to be input in AQWA with the MDIN card (ANSYS Inc 2012). Corresponding to $C_{dv} = 2.0$, $\frac{1}{2}\rho C_{dv} A$ is $3.40 \times 10^4 \text{ N}/(\text{m/s})^2$. The linear friction (viscous) damping is not significant compared to the quadratic viscous damping and is usually negligible in simulations (Orcina Ltd 2016). According to Batchelor (1973) and Telionis (1981), based on the frequency parameter β

$$\beta = \frac{D^2 \omega}{2\pi \nu} \quad (13)$$

friction damping coefficient is

$$B_v(friction) = \pi^{1.5} T \mu \beta^{0.5} \quad (14)$$

or

$$C_{dv}(friction) = 6\pi^2 \frac{T}{D} \cdot \frac{1}{KC \sqrt{4\pi\beta}} \quad (15)$$

In the next section, we will check the viscous damping influence on the inside cylinder of radius 3.25 m. In that case the diameter of the cylinder $D=6.5$ m, the draft of the cylinder $T=10.97$ m, $KC \in [0.58,1.06]$ (with quadratic damping) and $\beta \approx 3.63 \times 10^6$. If water viscosity is evaluated at 5°C, then $\mu = 1.519 \times 10^{-3} \text{ Pa} \cdot \text{s}$ and $\nu = 1.519 \times 10^{-6} \text{ m}^2/\text{s}$. $B_v(friction)$ is about 0.18 kPa·s, which is always below 1% of the linear damping applied ($B > 20 \text{ kPa} \cdot \text{s}$). $C_{dv}(friction) < 0.03$, which is always below 1.5% of the quadratic damping coefficient ($C_{dv} = 2.00$) proposed.

Other than that, the bearing connecting the two bodies inevitably involves mechanical/air frictions (damping). However, they should be smaller than the dominating ones (PTO force and viscous damping). In addition, since they accompany any PTO, it is fair to compare different PTOs without explicitly accounting them.

In general, the dominating damping is the potential damping, the linear damping from the PTO (as an input variable in AQWA) and the quadratic viscous damping (as a constant in AQWA).

5. Results and comparisons

5.1 Pneumatic PTO

The maximum power take off using air turbine in the cylindrical OWC has been studied by Wang and Falzarano (2013). The study used linear assumptions in air compression/decompression. If the turbine constant C_t is defined as

$$C_t = \frac{Q_t}{p} \quad (16)$$

p is the pressure drop across the turbine. Q_t is the airflow rate through the turbine. C_t is similar to the linear damping B in that both of them are ratios between the force and the velocity. The following equation of volume fluxes (across the horizontal cross section of the cylinder) holds in an adiabatic process

$$Q^S - \frac{i\omega p}{\rho g} Q^R = C_t \cdot p + \frac{V_c}{\kappa p_a} \cdot p \cdot (-i\omega) \quad (17)$$

Q^S is the scattering volume flux; $i\omega p Q^R / \rho g$ is the radiation volume flux; p is the dynamic air pressure. These variables are all of complex magnitude. Constant κ is the adiabatic index, which is 1.4 for air. Wang and Falzarano (2013) have derived that the power output through the airflow is

$$P_t = \frac{1}{2} [Re(p)Re(C_t \cdot p) + Im(p)Im(C_t \cdot p)] \quad (18)$$

Please note that P_t is the power that drives the turbine, it's the theoretical potential (maximum output) of the pneumatic PTO.

On the other hand, Wang and Falzarano (2017) have developed a method to calculate the wave energy deficit in a control boundary of a 3-D wave field. Applying the method, it is found that the energy output calculated from Eq. (18) always strictly matches the wave field energy deficit. The consistency serves as a solid validation of the power output calculation for the pneumatic system, showing what we calculated is indeed the maximum output of the pneumatic PTO. Since it is the verification tool for this study and gives us exactly the same results when Eq. (18) is used, the method will not be elaborated in this paper. However, details of the wave energy deficit derivation can be found in the paper by Wang and Falzarano (2017).

Application of control system can add or eliminate the imaginary part (phase change) to both PTOs, so the two PTOs are compared when they are in their common statuses (real turbine constant and real linear damping). In addition, the phase lag (induced by the imaginary part of the turbine constant) should be relatively small for actual turbines. Fig. 8 shows that the pneumatic PTO with real turbine constant outputs maximum power of 15.7 kW in this sea state.

5.2 Hydrodynamic PTO

To make sure that AQWA generates accurate incident wave, ZRON option is activated in AQWA-NAUT to output the relative (to the free surface) COG position. Fig. 9 shows the wave height (0.93 m) modeled exactly in AQWA-NAUT. The difference between the COG position time series and the relative (to the free surface) COG position time series is the incident wave elevation.

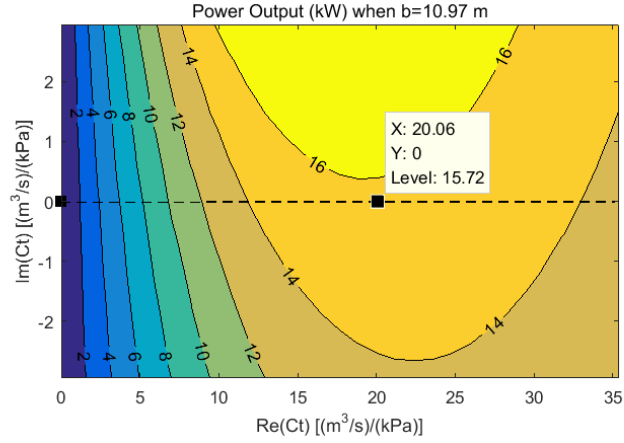


Fig. 8 Pneumatic power take off optimization

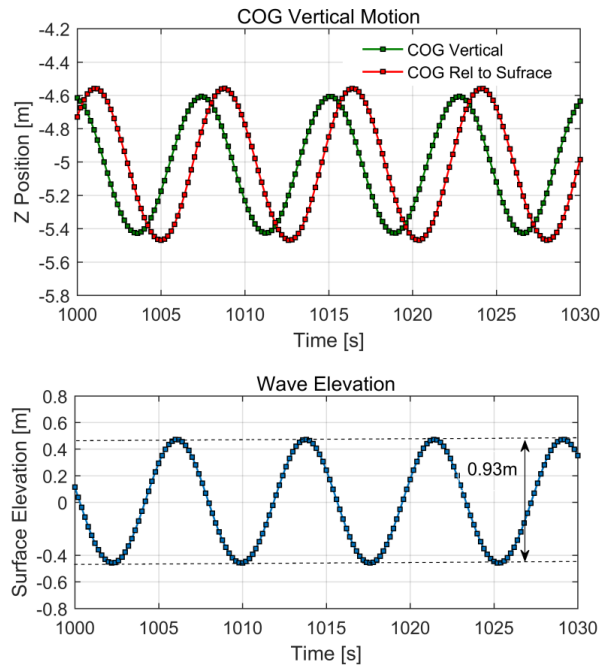


Fig. 9 Extracting wave elevation from AQWA-NAUT

Based on the definition of linear damping, we can calculate the average power of the MDL WEC

$$\bar{P} = \frac{B}{t_2 - t_1} \int_{t_1}^{t_2} \dot{z}(t)^2 dt \tag{19}$$

t_1 and t_2 is the start and end of a period long enough for the system to work in steady state, respectively. Fig. 10 shows the optimization of the hydrodynamic PTO.

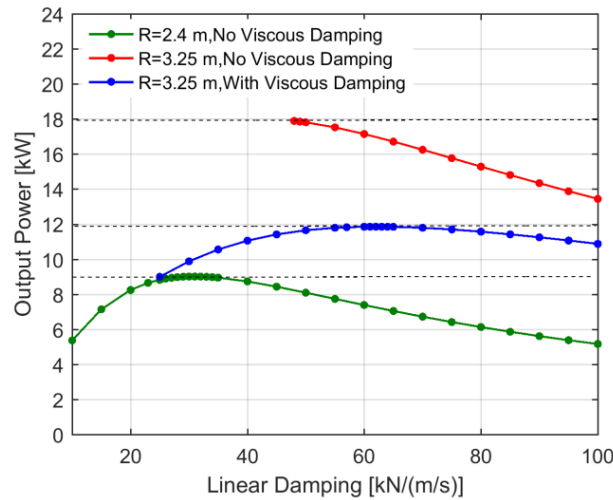


Fig. 10 Hydrodynamic power take off optimization

We need to point out that the 3.25 m radius case is not analyzed under smaller linear damping (electromagnetic load). When the damping is too small, motions at some time steps simulated in AQWA-NAUT vary too fast versus time, which incurs convergence warnings from AQWA. AQWA also does not allow the internal cylinder to be too close to the outside hollow cylinder, so the maximum power is estimated based on the largest radius modeled (3.25 m). Before comparing the pneumatic PTO with the hydrodynamic PTO, the following observations from Fig. 9 and Fig. 10 are marked :

- 1) Without viscous damping, the theoretical maximum output power from the hydrodynamic PTO is about 17.9 kW, about 14% higher than the pneumatic PTO;
- 2) Increasing radius of the inside cylinder helps increase the theoretical wave energy output;
- 3) With conservative viscous damping estimation, the energy output drops by 35% (from about 17.9 kW to about 12 kW) at most; the load that optimizes the power output with viscous damping may not coincident with the load that optimizes the power output without viscous damping.

5.3 Efficiency (in practice) comparison

In this subsection, some comparisons are made between the two PTOs based on the simulations and theoretical calculations in the subsection 5.1 and 5.2. We are not able to get the absolute efficiencies of the two PTOs (since many uncertainties are involved), but by observing their working processes, it is possible to compare their relative efficiencies. Fig. 11 shows different processes of the two PTOs. Wave energy transfers from the incident wave to the water heave motion (1P or 1H) are similar for the two PTOs. The pneumatic PTO uses air as an internal media to convert fluid motion to solid rotation, which introduces one more stage than the hydrodynamic PTO. One issue for the pneumatic PTO is that the efficiency of converting the airflow energy to the mechanical energy can hardly reach more than 50%, evident by both CFD simulations (Cui and Hyun 2016) and experimental results (Okuhara *et al.* 2013). In addition, that doesn't include the

influence from non-adiabatic process in the air compression and decompression cycle (2P). The compression heats the air but the heated air is pushed out of the air chamber. Besides, the air has continuous heat exchange with the OWC structure as well as water. Considering the second law of thermodynamics, it should be a process with inevitable energy dissipations.

Table 5 shows the efficiency estimates for the two PTOs, in which similar stage(s) has been put in the same line. Though an accurate estimation of the process 2P cannot be given in this study, process 2P surely adds to the energy loss of 3P (>50% loss). The stage 4P and 3H involve similar mechanical frictions. However, since this part is relative small (and needs to be kept small), its effect is not accounted quantitatively.

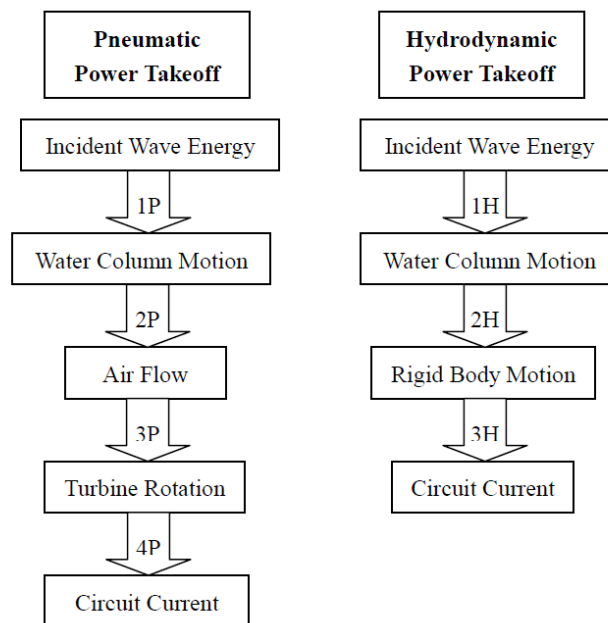


Fig. 11 Flow chart of different OWC power take off

Table 5 Efficiency estimates for PTOs

Pneumatic		Comparison	Hydrodynamic	
Stage	Power Variation		Stage	Power Variation
1P	(+) Capture width	H-P (about 14%)	1H	(+) Capture width
	(-) Viscous loss	Similar		(-) Viscous loss
2P	(-) Non-adiabatic loss	H-P (>15%)	2H	(-) Viscous damping
3P	(-) Turbine efficiency		3H	(-) Mechanical loss
4P	(-) Mechanical loss	Relative Small		

Table 5 attempts to evaluate the efficiencies of the two PTOs under particular parameters. Based on observation 1) in subsection 5.2, the process 1P is estimated to have 14% advantage over the process 1H. Though observation 1) in subsection 5.2 is when the viscous loss (which makes the wave elevation inside the hollow cylinder smaller than our calculation) is not considered, we can stick to the 14% estimation since the viscous loss in the two scenarios are quite similar. The process 2P (loss inevitable, >0%) and 3P (loss >50%) combined yield more than 50% power loss while the process 2H yields 35% power loss (in its worst situation) based on observation 3) in subsection 5.2. So the process 2H will be >15% more efficient than the process (2P+3P). It needs to be mentioned that conservative (larger) viscous damping has been used in estimating the efficiency of the process 2H. Table 5 indicates that the hydrodynamic PTO under these design parameters outputs at least 29% more energy.

In the case analyzed, energy captured theoretically is 15.7 kW for the pneumatic PTO versus 17.9 kW (about 14% larger) for the hydrodynamic PTO.

Actual captured energy after 3P and 2H is 7.8 kW for the pneumatic PTO versus 11.9 kW (about 52% larger) for the hydrodynamic PTO.

6. Conclusions

In the study, we modified the traditional OWC system by changing the pneumatic PTO to the hydrodynamic PTO, which turns out to be a design that takes advantage of the two-body interaction. After looking into the governing equations, we explored the feasibility of simulating this WEC design with the AQWA suite. The results show that we can implement a linear damping to represent the electromagnetic force when two important parameters are within certain range.

AQWA is used to explore the maximum output of the hydrodynamic PTO when viscous damping (estimated from the model tests for the heaving cylinder) is considered. In parallel, the maximum output of the pneumatic PTO is calculated using the linear assumptions in air compression/decompression. By going through the working processes of the two PTOs, we compared their relative practical efficiencies. In general, the hydrodynamic PTO appears to be more efficient than the pneumatic PTO. Based on our calculations, the hydrodynamic PTO can capture >14% more energy than the pneumatic PTO theoretically. Considering other processes in the energy conversion, the hydrodynamic PTO can be >29% more efficient than the pneumatic PTO.

As we can see, the hydrodynamic PTO is worthy of further study. However, since parts of the study involve nonlinearity, AQWA can only be used as a tool for primary investigations on the potential of different WEC designs. In our future work, a more advanced tool will be developed specifically for WEC simulations. With that tool, the PTO forces, the control forces and the nonlinear (large amplitude) motions are expected to be modeled more precisely.

Acknowledgements

The authors would like to acknowledge the Marine Dynamics Laboratory (MDL) at Texas A&M University. In addition, Prof. Huang from Texas A&M University Electrical Engineering department has provided valuable suggestions on power take off study. This work has been supported by INTECSEA Inc headquartered in Houston as a research project.

References

- AQWA-LINE User Manual, (2011a), ANSYS Inc, Houston, USA.
- AQWA-DRIFT User Manual, (2011b), ANSYS Inc, Houston, USA.
- AQWA-NAUT User Manual, (2011c), ANSYS Inc, Houston, USA.
- AQWA Reference Manual, (2012), ANSYS Inc, Houston, USA.
- Bard, J. and Kracht, P. (2013), "Report on linear generator systems for wave energy converters", Fraunhofer Institute for Wind Energy and Energy System Engineering. http://www.sdwed.civil.aau.dk/digitalAssets/97/97525_d3.2.pdf.
- Batchelor, G.K. (1973), *An Introduction to Fluid Dynamics*, Cambridge University Press, London.
- Cho, I.H., Kim, M.H. and Kweon, H.M. (2012), "Wave energy converter by using relative heave motion between buoy and inner dynamic system", *Ocean Syst. Eng.*, **2**(4), 297-314.
- Cho, I.H. and Kim, M.H. (2017), "Hydrodynamic performance of a wave energy converter with two concentric vertical cylinders by analytic solutions and model tests", *Ocean Eng.*, **130**, 498-509.
- Cozijn, H., Uittenbogaard, R. and Brake, E. (2005), "Heave roll and pitch damping of a deepwater CALM buoy with a skirt", *Proceedings of the 15th Int. Offshore Polar Eng. Conf.*, Seoul, June.
- Cui, Y. and Hyun, B.S. (2016), "Numerical study on wells turbine with penetrating blade tip treatments for wave energy conversion", *Int J. Naval Arch. Ocean Eng.*, **8**, 456-465.
- Drew, B., Plummer, A. and Sahinkaya, M. (2009), "A review of wave energy converter technology", *Proc. of the Inst. of Mech. Eng., Part A: J. of Power and Energy*, **223**(8), 887-902.
- Evans, D.V. and Porter, R. (1997), "Efficient calculation of hydrodynamic properties of OWC-type devices", *J. Offshore Mech. Arct.*, **119**, 210-218.
- Falnes, F. (2002), *Ocean Waves and Oscillating Systems*, Cambridge University Press, Cambridge, UK.
- Falzarano, J.F. et al. (2012), "Offshore renewable energy", *Proceedings of the 18th Int. Ship and Offshore Struct. Congr.*, Rostock, Germany.
- Garriga, O. and Falzarano, J.F. (2008), "Water wave interaction on a truncated vertical cylinder", *J. Offshore Mech. Arct.*, **130**(3), 1-8.
- Guha, A. (2016), *Development and application of a potential flow computer program: Determining first and second order wave forces at zero and forward speed in deep and intermediate water depth*, PhD Thesis, Texas A&M University, College Station, USA.
- Liu, Y. and Falzarano, J.F. (2016), "Irregular frequency removal methods: theory and applications in hydrodynamics", *Mar. Syst. Ocean Technol.*, **10**(1), 1-16.
- Liu, Y. and Falzarano, J.F. (2017), "A method to remove irregular frequencies and log singularity evaluation in wave-body interaction problems", *J. Ocean Eng. Mar. Energy*, **3**(2), 161-189.
- López, I., Andreua, J., Ceballos, S., Alegría, I.M. and Kortabarria, I. (2013), "Review of wave energy technologies and the necessary power-equipment", *Renew. Sust. Energ. Rev.*, **27**, 413-434.
- Molin, B. (2001), "On the piston and sloshing modes in moonpools", *J. Fluid Mech.*, **430**, 27-50.
- OrcaFlex Documentation, (2016), Orcina Ltd, Ulverston, UK. <http://www.orcina.com/Software/Products/OrcaFlex/Documentation/Help>.
- Okuhara, S., Takao, M., Takami, A. and Setoguchi, T. (2013), "Wells turbine for wave energy conversion improvement of the performance by means of impulse turbine for bi-directional flow", *Open J. Fluid Dynam.*, **3**, 36-41.
- Schwartz, D. and Mentzer, A. (2016), "Linear induction basics", <http://linearinductionwavepower.weebly.com/linear-point-absorbers.html>.
- Somayajula, A. and Falzarano, J.F. (2015), "Large-amplitude time-domain simulation tool for marine and offshore motion prediction", *Mar. Syst. Ocean Technol.*, **10**(1), 1-17.
- Tao, L., Cheng, L. and Thiagarajan, K. (1999), "Numerical estimation of hydrodynamic heave damping of a vertical cylinder with appendages", *Proceedings of the 9th Int. Offshore and Polar Eng. Conf.*, Brest, May.

- Thiagarajan, K. and Troesch, A. (1994), "Hydrodynamic heave damping estimation and scaling for tension leg platforms", *J. Offshore Mech. Arct.*, **116**(2), 70-76.
- Thorburn, K. and Leijon, M. (2007), "Farm size comparison with analytical model of linear generator wave energy converters", *Ocean Eng.*, **34**(5-6), 908-916.
- Telionis, D.P. (1981), *Unsteady Viscous Flows*, Springer-Verlag, New York, NY.
- Wang, H. (2013), *Wave energy extraction from an oscillating water column in a truncated circular cylinder*, Master Thesis, Texas A&M University, College Station, USA.
- Wang, H. and Falzarano, J.F. (2013), "Energy extraction from the motion of an oscillating water column", *Ocean Syst. Eng.*, **3**(4), 327-348.
- Wang, H. and Falzarano, J.F. (2017), "Energy balance analysis method in oscillating type wave converter", *J. Ocean Eng. Mar. Energy*, 1-16. doi:10.1007/s40722-017-0081-y
- Yang, S., Lee, S., Park, J., Han, S., Choi, Y., Do, J., Kwon, S. and Molin, B. (2016), "Experimental study on piston-and sloshing-mode moonpool resonances", *J. Mar. Sci. Techno.*, **21**(4), 715-728.
- Zheng, Z., Huang, P., Gao, D. and Chang, Z. (2015), "Analysis of electromagnetic force of the linear generator in point absorber wave energy converters", *J. Mar. Sci. Tech.*, **23**, 475-480.

MK